INTEGRATED GAS DYNAMIC AND THERMODYNAMIC COMPUTATIONAL MODELING OF MULTICYLINDER 4-STROKE SPARK IGNITION ENGINE USING GASOLINE AS A FUEL

by

Jeevan V. TIRKEY, Hari N. GUPTA, and Shailendra K. SHUKLA

Original scientific paper
UDC: 621.43.05:517.95
DOI: 10.2298/TSCI0903113T

This paper presents a computational tool for the evaluation of engine performance and exhaust emissions for four stroke multi-cylinder spark ignition engine which uses gasoline as a fuel. Gas dynamics flow in multi-cylinder intake and exhaust systems are modeled by using one-dimensional unsteady compressible flow equations. The hyperbolic partial differential equations are transferred into a set of ordinary differential equations by using method of characteristics and solved by finite difference method. Compatibility relationships between local fluid velocity and sonic velocity are expressed in terms of Riemann variables, which are constant along the position characteristics. The equations are solved numerically by using rectangular grid in the flow direction and time. In this model nitric oxide concentration is predicted by using the rate kinetic model in the power cycle and along the exhaust pipes. Carbon monoxide is computed under chemical equilibrium condition and then empirical adjustment is made for kinetic behaviors based upon experimental results. A good agreement is obtained in the comparison of computed and experimental results of instantaneous cylinder pressure, manifold pressure and temperature, and nitric oxide and carbon monoxide emissions level.

Key words: *computer simulation, method of characteristics, Riemann variables, non-homentropic, rate kinetics, exhaust species*

Introduction

In recent years, the internal combustion engine powered vehicles have come under heavy attack due to environment pollution through exhaust emissions of mainly the oxides of nitrogen (NO_x), carbon monoxide (CO), and unburned hydrocarbons (HC). It has a deleterious effect on human beings and plants. So to achieve a clean environment, better understanding and modifications of the combustion process are necessary. At the same time, the fluid dynamic process is much important for determining the overall performance of internal combustion engine throughout its operating range.

In this respect computerized simulation techniques have been tried in recent years to study the various parameters of engine performance and exhaust pollutant emissions, rather than performing the experiments by using a real engine.

Abd Alla [1] has offered simulation modeling for single cylinder engine, which provides the correlation of heat release rate formula to predict the cylinder pressure that can be used to find indicated power and other performances for engine. Kodah *et al.* [2], constructed a theoretical model to predict the cylinder's gas pressure, temperature, and rate of heat release. Raine

et al. [3] have simulated and verified the result with measured values from single cylinder engine by using "power gas" as a fuel. The power gas is a synthetic fuel consisted mainly of carbon monoxide and hydrogen. The "power gas" fuel engine emits higher CO_2 and low CO in comparison to compressed natural gas (CNG) and gasoline. Gasoline fuel operated engine provides higher volumetric efficiency in comparison to CNG and "power gas" fuel. In this connection Bayraktar [4] presented a mathematical SI engine cycle and combustion model and discussed that liquid petroleum gas (LPG) fueled engine gives negative effect on engine performance, fuel economy, and engine structural elements, when it is used at the same fuel-air equivalence ratio as gasoline. However, it has positive effects on obnoxious exhaust emissions such as CO and NO. Kultar *et al.* [5] simulated and confirmed with experimental values for single cylinder engine that, efficiency decreases more at part throttle condition in comparison to wide open throttle (WOT). Partially open throttle valve leads to increase in pumping loss, resulting reduction of pressure loop in *p-v* diagram. Adams *et al.* [6] analyzed and tested with the variable compression ratio engine and suggested that significant saving in fuel consumption can be attained by varying the compression ratio as a function of load and engine speed in comparison to an engine with a constant compression ratio.

It has been studied [5, 7-9] that, if a gasoline or alternative fueled engine can be run on a very lean air fuel mixture, the combustion process will become more complete, and the level of exhaust emissions of CO, HC, and NO_x will be significantly reduced. However, it is normally not possible to run a conventional carburetted engine on such a lean mixture, because a normal carburettor produces a wet, non-homogenous mixture and the fuel is unevenly distributed between the inlet manifold branches. Thus in multicylinder engine, some cylinders receive a much leaner mixture than others, and misfiring occurs in the lean cylinders if the overall mixture is beyond a certain limit.

Kesgin [9] studied about intake and exhaust pipe size as well as inlet and exhaust valve of a stationary natural gas engine performance. The effect of pipe elongation and T junction in exhaust pipe offers an improvement potential of the engine efficiency, but this is limited because of the compactness of engine size. The intake and exhaust manifold systems determine the engine operation behavior in steady and transient modes, the engine performance and the engine emissions regarding exhaust gas and sound.

In continuation of the process undertaken, zero and quasi dimensional modeling have been developed [9-14] for single cylinder engine to simulate four stroke cycle of a spark ignition engine fueled with fuel as gasoline, ethanol, hydrogen, LPG, and their mixture. The study has been performed to investigate combustion cycle, pollution emission and performance for various engine geometric operational condition and fuel.

Most practical stimulation of intake and exhaust manifold are based on one dimensional compressible flow equations and ideal gas behavior. The classic method to attempt to solve the one dimensional unsteady governing equation is through the use of method of characteristic (MOC) and finite difference method (FDM) [9, 15-17].

Regarding this recent view there is a lack of experimental verification on multicylinder engine including gas dynamic effect in inlet and exhaust manifolds. In this paper attempt is made to investigate the multicylinder (4 cylinders) SI engine's combustion process, cycle performance at various operating conditions, and engine manifold's gas exchange system.

For practical and reliable evaluation, a quasi dimensional SI engine cycle computer simulation model has been developed, including intake and exhaust manifold system. In this model compressible characteristic of flow is analyzed by applying MOC model on relevant base of gas dynamic, thermodynamic, and chemical kinetic. With this technique hyperbolic partial differential equations are transformed into ordinary differential equations that apply on charac-

teristic lines. The transformed equations are solved by FDM using interpolation onto a rectangular grid.

To check the reliability of the present model, comparisons of results with experimental work that have been presented.

Finally, the manifold gas dynamic effects on intake and exhaust ports pressure, pipe line pressure, and temperature are explored. The further application of this model is to use alternative fuel engine, examining the effect of engine design and operating parameters.

Power cycle calculation

Power cycle occurs when both inlet and exhaust valves are closed. It consists of the following processes:

– compression,
– ignition and propagation of flame front, and
– expansion: (1) two zone, (2) full products.

Compression. The compression process starts at the trapped condition. The state of the gas at this point is derived using a perfect mixing model for the induced fresh charge and residual from the previous cycle. Reactions are neglected during compression and a perfect gas mixture is assumed.

First law of thermodynamics to the cylinder charge and equation of state gives the relations:

$$\frac{\mathrm{d}p}{\mathrm{d}\alpha} \quad \frac{R}{C_\mathrm{v}} \frac{\mathrm{d}Q}{\mathrm{d}\alpha} \quad \frac{p\mathrm{d}V}{\mathrm{d}\alpha} \frac{R}{C_\mathrm{v}} \quad 1 \quad \frac{1}{V} \tag{1}$$

For unburned mixture denoted by suffix "m":

$$\frac{\mathrm{d}T_\mathrm{m}}{\mathrm{d}\alpha} \quad T_\mathrm{m} \frac{1}{V}\frac{\mathrm{d}V}{\mathrm{d}\alpha} \quad \frac{1}{p}\frac{\mathrm{d}p}{\mathrm{d}\alpha} \tag{2}$$

Convective heat transfer from the gas to wall is calculated by using Annand's equation [10-12].

$$\frac{q}{F} \quad a\frac{k_\mathrm{q}}{D}(\mathrm{Re})^b (T_\mathrm{m} \quad T_\mathrm{w}) \quad c(T_\mathrm{m}^4 \quad T_\mathrm{w}^4) \tag{3}$$

where k_q is the thermal conductivity (= $c_\mathrm{p}\mu/0.7$), and a, b, and c are constants (a = 0.4, b = 0.7, $c = 4.3\cdot10^{-9}$).

Reversible work done by reciprocating piston is:

$$\frac{\mathrm{d}W}{\mathrm{d}\alpha} \quad p\frac{\mathrm{d}V}{\mathrm{d}\alpha} \tag{4}$$

As the compression process continues the variables are incremented by following equation and solved by the fourth order Runge-Kutta method:

$$X_{n\ 1} \quad X_\mathrm{n} \quad \frac{\mathrm{d}X}{\mathrm{d}\alpha}\Delta\alpha \tag{5}$$

where "X" is any variable.

Ignition. The laminar flame speed for gasoline at pressure, temperature, and equivalence ratio which occurs in engine have been calculated by using the correlation of Metghalchi and Keck's [4, 11, 17],

Laminar flame speed (S_L), is:

$$S_L \quad S_{us} \left(\frac{T_u}{T_{us}}\right)^{\alpha} \left(\frac{p}{p_{us}}\right)^{\beta} \text{ [cm/s]} \tag{6a}$$

where the reference pressure and temperature are $p_{us} = 1$ atm, and $T_{us} = 300$ K, respectively. S_{us} is the burning velocity at p_{us} and T_{us}. α and β as well as S_{us}, are functions of Φ and are given by [17]:

$$\begin{aligned} S_{us} &\quad 30.5 \quad 54.9(\Phi \quad 1.21)^2 \text{ [cm/s]} \\ \alpha = 2.4 &\quad 0.271\Phi^{3.51}, \quad \beta \quad 0.357 \quad 0.14\Phi^{2.77} \end{aligned} \tag{6b}$$

The first value of product temperature and pressure is guessed by following expressions developed by Annand [18]:

$$T_p = T_m + 2500.0\,\Phi f_i \text{ for } \Phi \quad 1.0 \tag{7a}$$

$$T_p = T_m + 2500.0\,\Phi f_i - 700(\Phi - 1.0) f_i \text{ for } \Phi > 1.0 \tag{7b}$$

This first product temperature (T_p) is calculated by balancing the specific internal energy of product at the guessed temperature with that of unburned mixture at current unburned temperature using an iterative technique.

The turbulent flame front speed (S_p) is calculated by [11, 12]:

$$S_T \quad S_L Ff \frac{\dfrac{\rho_u}{\rho_b}}{\dfrac{\rho_u}{\rho_b} \quad 1 \; X_b \quad 1} \tag{8}$$

where, flame factor $Ff = 1 + 0.00018\,RPM$, and X_b is burned mass fraction [2, 12].

Mass burning rate is calculated by [11, 12, 17]:

$$\frac{dm_b}{dt} \quad A_f \rho_u S_T \tag{9}$$

Flame front areas are calculated on the basis of geometrical model. The flame front radius (R) and delay period ($\Delta\theta$) are calculated by the relationships [11, 12, 18]:

$$R \quad \frac{\Delta\theta S_T}{6RPM}, \quad \Delta\theta \quad \frac{6RPM}{S_T} \frac{0.0001 V_{cyl}}{\pi} \tag{10a, b}$$

In order to initiate the two zones (burned & unburned) a finite product volume $V_p = 10^{-3}$ = cylinder volume, is assumed.

For two zone calculation [18] a three sequential steps are adopted which are depicted in fig. 1.

In process A (fig. 1), it is assumed that cylinder content (unburned m mixture) undergoes compression (V_1 to V_2) with heat loss dQ_m (combustion is not initiated).

The condition at the end of this process becomes:

$$T_m \quad T_{m_1} \left(\frac{V_1}{V_2}\right)^{\frac{R_m}{C_{vm}}} \quad \frac{dQ_m}{mc_{v_m}} \tag{11}$$

$$p \quad \frac{p_1 V_1 T_m}{V_2 T_{m_1}} \tag{12}$$

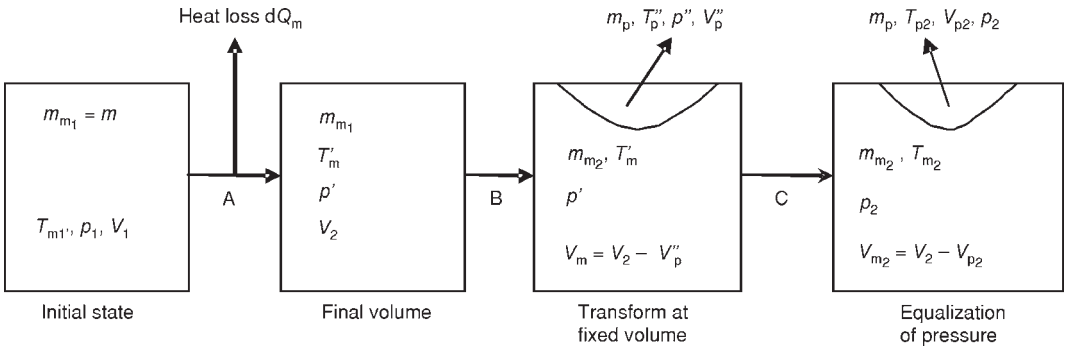

Figure 1

In process B (fig. 1), the assumption is that the flame nucleus is formed by constant specific volume combustion, which results in a high pressure and temperature in the products region. During the process T'_m and p' are kept fixed.

Temperature of the product in the flame nuclease (T_p) and pressure in the flame kernel can be calculated as:

$$p \quad \frac{R_p T_p}{R_m T_m} p \tag{13}$$

and the mass of product is:

$$m_p \quad \frac{2\pi r^3}{3V_2} m \tag{14}$$

where m is the total mass trapped in the cylinder. Mass of the mixture remaining after process B is:

$$m_{m_2} \quad m \quad m_p \tag{15}$$

Total internal energy

$$U \quad mu_m \quad m_{m_2} u_m \quad m_p u_p \tag{16}$$

Process C (fig. 1) – pressure equalization, equating the total internal energy before and after process C:

$$m_{m_2} u_m \quad m_p u_p \quad m_{m_2} u_{m_2} \quad m_p u_{p_2} \tag{17}$$

For reversible adiabatic process hold:

$$\frac{T_{m_2}}{T_m} \quad \frac{p_2}{p}^{\frac{k_m \ 1}{k_m}} \tag{18}$$

and

$$\frac{T_{p_2}}{T_p} \quad \frac{p_2}{p}^{\frac{k_p \ 1}{k_p}} \tag{19}$$

also

$$\frac{p_2}{p} \quad \frac{p_2}{p}\frac{p}{p} \quad \frac{p_2}{p}\frac{R_m t_m}{R_p t_p} \tag{20}$$

Using eqs. (17), (18), and (20) the following relation is obtained:

$$\psi - 1 = A(1 - B\psi^{\alpha}) \tag{21}$$

where $\psi = T_{m_2}/T_m$, and $\alpha = [k_m/(k_m - 1)][(k_p - 1)/k_p]$

$$A \quad \frac{m_{\mathrm{p}} c_{\mathrm{v_p}} T_{\mathrm{p}}}{m_{\mathrm{m_2}} c_{\mathrm{v_m}} T_{\mathrm{m}}}, \quad B \quad \frac{R_{\mathrm{m}} T_{\mathrm{m}}}{R_{\mathrm{p}} T_{\mathrm{p}}}^{\frac{k_{\mathrm{p}} \; 1}{k_{\mathrm{p}}}}$$

The eq. (21) can be solved for ψ with an iterative technique.

Expansion with two zones. In this model charges are considered homogeneous, pressure is uniform throughout the cylinder, volume occupied by the flame reaction zone is negligible, burned gas is at full thermodynamic equilibrium except for the NO_x, and there is no heat transfer between burned and unburned zones. The temperature and pressure of the burned and unburned mixture can be obtained by applying the first law of thermodynamics, energy equation, flame speed, and the geometry of the burned zone in relation to the combustion chamber [12, 18]:

$$\frac{\mathrm{d}T_{\mathrm{m}}}{\mathrm{d}\alpha} \quad \frac{V_{\mathrm{m}}}{m_{\mathrm{m}} c_{\mathrm{p_m}}} \frac{\mathrm{d}P}{\mathrm{d}\alpha} \quad \frac{1}{m_{\mathrm{m}} c_{\mathrm{p_m}}} \frac{\mathrm{d}Q_{\mathrm{m}}}{\mathrm{d}\alpha} \tag{22}$$

$$\frac{\mathrm{d}T_{\mathrm{p}}}{\mathrm{d}\alpha} \quad \frac{p}{m_{\mathrm{p}} R_{\mathrm{p}}} \frac{\mathrm{d}V}{\mathrm{d}\alpha} \quad \frac{R_{\mathrm{p}} T_{\mathrm{p}}}{p} \quad \frac{R_{\mathrm{m}} T_{\mathrm{m}}}{p} \frac{\mathrm{d}m_{\mathrm{p}}}{\mathrm{d}\alpha} \quad \frac{R_{\mathrm{m}} V_{\mathrm{m}}}{p c_{\mathrm{p_m}}} \frac{\mathrm{d}p}{\mathrm{d}\alpha} \quad \frac{R_{\mathrm{m}}}{p c_{\mathrm{p_m}}} \frac{\mathrm{d}Q_{\mathrm{m}}}{\mathrm{d}\alpha} \quad \frac{V \mathrm{d}p}{p \mathrm{d}\alpha} \tag{23}$$

$$\frac{\mathrm{d}p}{\mathrm{d}\alpha} \quad \frac{1 \quad \frac{c_{\mathrm{v_m}}}{R_{\mathrm{p}}} \; p \frac{\mathrm{d}V}{\mathrm{d}\alpha} \quad (u_{\mathrm{p}} \quad u_{\mathrm{m}}) \; c_{\mathrm{v_p}} \; T_{\mathrm{p}} \quad \frac{R_{\mathrm{m}}}{R_{\mathrm{p}}} T_{\mathrm{m}} \quad \frac{\mathrm{d}m_{\mathrm{p}}}{\mathrm{d}\alpha}}{\frac{c_{\mathrm{v_m}}}{c_{\mathrm{p_m}}} \quad \frac{c_{\mathrm{v_p}}}{R_{\mathrm{p}}} \frac{R_{\mathrm{m}}}{c_{\mathrm{p_m}}} \quad \frac{dQ_{\mathrm{m}}}{\mathrm{d}\alpha} \quad \frac{\mathrm{d}Q}{\mathrm{d}\alpha} \quad \frac{c_{\mathrm{v_p}}}{c_{\mathrm{p_m}}} \frac{R_{\mathrm{m}}}{R_{\mathrm{p}}} V_{\mathrm{m}} \quad \frac{c_{\mathrm{v_m}}}{c_{\mathrm{p_m}}} V_{\mathrm{m}} \quad \frac{c_{\mathrm{v_p}}}{R_{\mathrm{p}}} V} \tag{24}$$

The variables are incremented by the Runge-Kutta method. Theoretically combustion should terminate when V_{m} 0. In our numerical solution, it is assumed to terminate at the beginning of the time step where we find that the current value of V_{m} is just negative.

Once the combustion is complete the variables are organized to calculate for singe zone only. The Runge-Kutta method is used. Heat transfer rate is calculated by Annand's equation.

Gas exchange

The gas exchange period is the duration between opening of the exhaust valve and closing of the inlet valve, when either one or both valves are open. A homogeneous mixture is assumed for the residual gases mixing with the fresh charge. The gas exchange calculations are carried out with the average gas properties of the resulting mixture.

By applying the first law of thermodynamics, the energy equation for the gas exchange period is [18, 19]:

$$d\dot{Q} \quad \mathrm{d}\dot{W} \quad \frac{\partial}{\partial t}(m_{\mathrm{c}} u_{\mathrm{c}}) \quad \mathrm{d}\dot{m}_{\mathrm{e}} h e_0 \quad \mathrm{d}\dot{m}_{\mathrm{i}} h i_0 \tag{25}$$

Stagnation enthalpy $h_0 = a_0^2/(k-1)$ and internal energy $m_{\mathrm{c}} u_{\mathrm{c}} = p_{\mathrm{c}} V_{\mathrm{c}}/(k-1)$ after rearranging the eq. (25) becomes:

$$\frac{V_c}{k_c - 1}\frac{dp_c}{d\alpha} \quad \frac{k_c}{k_c - 1} p_c \frac{dV_c}{d\alpha} \quad \frac{a_{i_0}^2}{k_i - 1}\frac{dm_i}{d\alpha} \quad \frac{a_{e_0}^2}{k_e - 1}\frac{dm_e}{d\alpha} \quad \frac{dQ}{d\alpha} \tag{26}$$

The mass balance in the cylinder is:

$$\frac{dm_c}{d\alpha} \quad \frac{dm_i}{d\alpha} \quad \frac{dm_c}{d\alpha} \tag{27}$$

$$(m_c)_{n+1} \quad (mc)_n \quad \frac{dm_c}{d\alpha}\Delta\alpha \tag{28}$$

$$(p_c)_{n+1} \quad (pc)_n \quad \frac{dp_c}{d\alpha}\Delta\alpha \tag{29}$$

$$(T_c)_{n+1} \quad \frac{p_c V_c}{R m_c}_{n+1} \tag{30}$$

Pipe calculations

The partial differential equations for 1-D non-steady flow of a perfect gas in a duct with gradual area change, wall friction, heat transfer, and entropy changes are [15, 16, 18]:

– continuity

$$\frac{\partial\rho}{\partial t} \quad \rho\frac{\partial u}{\partial x} \quad u\frac{\partial\rho}{\partial x} \quad \rho\frac{u}{F}\frac{dF}{dx} \quad 0 \tag{31}$$

– momentum

$$\frac{\partial u}{\partial t} \quad u\frac{\partial u}{\partial x} \quad \frac{1}{\rho}\frac{\partial p}{\partial x} \quad \frac{4f}{D}\frac{u^2}{2}\frac{u}{|u|} \quad 0 \tag{32}$$

where

$$f \quad \frac{\tau_w}{\frac{1}{2}\rho u^2}$$

– energy equation:

$$\frac{\partial p}{\partial t} \quad u\frac{\partial p}{\partial x} \quad a^2\frac{\partial\rho}{\partial t} \quad a^2 u\frac{\partial p}{\partial x} \quad (k-1)\rho q \quad u\frac{4f}{D}\frac{u^2}{2}\frac{u}{|u|} \quad 0 \tag{33}$$

where

$$a^2 \quad \frac{kp}{\rho}$$

The method of characteristics is applied to solve these equations. Using the Riemann variables, the characteristic solutions of these equations are [18]:

(a) λ *characteristics*

$$\lambda \quad A \quad \frac{k-1}{2}U \tag{34}$$

– direction condition

$$\frac{dX}{dZ} \quad U \quad A \tag{35}$$

– compatibility condition

$$d\lambda \quad dA \quad \frac{k-1}{2}dU \tag{36}$$

Taking non-dimensional parameter as:

$$A \quad \frac{a}{a_{\text{ref}}}, \quad U \quad \frac{u}{a_{\text{ref}}}, \quad A_{\text{a}} \quad \frac{a_{\text{A}}}{a_{\text{ref}}}, \quad Z \quad \frac{a_{\text{ref}} t}{x_{\text{ref}}}$$

$$\mathrm{d}\lambda \quad \frac{A}{A_{\text{a}}}\mathrm{d}A_{\text{a}} \quad \frac{(k \quad 1)^2}{2A} q \frac{x_{\text{ref}}}{a_{\text{ref}}^3}\mathrm{d}Z \quad \frac{k \quad 1}{2}\frac{AU}{F}\frac{\mathrm{d}F}{\mathrm{d}X}\mathrm{d}Z$$

$$\frac{k \quad 1}{2} 2f \frac{x_{\text{ref}}}{D} U^2 \frac{U}{|U|} \quad 1 \quad (k \quad 1)\frac{U}{A} \quad \mathrm{d}Z \tag{37}$$

(b) *β characteristics*

$$\beta \quad A \quad \frac{k \quad 1}{2} U \tag{38}$$

– direction condition

$$\frac{\mathrm{d}X}{\mathrm{d}Z} \quad U \quad A \tag{39}$$

– compatibility condition

$$\mathrm{d}\beta \quad \mathrm{d}A \quad \frac{k \quad 1}{2}\mathrm{d}U \tag{40}$$

$$\mathrm{d}\beta \quad \frac{A}{A_{\text{a}}}\mathrm{d}A_{\text{a}} \quad \frac{(k \quad 1)^2}{2A} q \frac{x_{\text{ref}}}{a_{\text{ref}}^3}\mathrm{d}Z \quad \frac{(k \quad 1)}{2}\frac{AU}{F}\frac{\mathrm{d}F}{\mathrm{d}X}\mathrm{d}Z$$

$$\frac{k \quad 1}{2} \quad 2f \frac{x_{\text{ref}}}{D} U^2 \frac{U}{|U|} \quad 1 \quad (k \quad 1)\frac{U}{A} \quad \mathrm{d}Z \tag{41}$$

In eqs. (37) and (41), the first term is the change in $\mathrm{d}\lambda$ (or $\mathrm{d}\beta$) due to entropy change, the second term is due to heat transfer, the third term is due to area changes and the fourth term is due to friction.

(c) Path line characteristics

– direction condition

$$\frac{\mathrm{d}X}{\mathrm{d}X} \quad U \quad \frac{\lambda \quad \beta}{k \quad 1} \tag{42}$$

– compatibility condition

$$\mathrm{d}A_{\text{a}} \quad \frac{k \quad 1}{2}\frac{A_{\text{a}}}{A^2} \quad \frac{qx_{\text{ref}}}{a_{\text{ref}}^3} \quad \frac{2fx_{\text{ref}}}{D}|U^3| \quad \mathrm{d}Z \tag{43}$$

The local Riemann variables, λ and β, and the entropy level A_{a} give the pressure, temperature, and velocity of the fluid at a point. The following relationships are used:

$$A \quad \frac{\lambda \quad \beta}{2}, \quad U \quad \frac{\lambda \quad \beta}{k \quad 1}$$

Considering these relationships and isentropic process eq. (43) becomes,

$$\mathrm{d}A_{\text{a}} \quad 2(k \quad 1)\frac{A_{\text{a}}}{(\lambda \quad \beta)^2} \quad \frac{qx_{\text{ref}}}{a_{\text{ref}}^3} \quad \frac{2fx_{\text{ref}}}{D}\left|\frac{\lambda \quad \beta}{k \quad 1}\right|^3 \quad \mathrm{d}Z \tag{44}$$

Equation (44) gives the change in entropy level of the gas particles along path lines. The relationship between the pressure and the speed of sound is given by:

$$\frac{p}{p_{\text{ref}}} \quad \frac{a}{a_{\text{A}}}^{\frac{2k}{k\ 1}} \quad \frac{A}{A_{\text{a}}}^{\frac{2k}{k\ 1}} \tag{45}$$

Heat transfer in pipes

The Reynolds analogy for heat transfer could be used with the method of characteristic to calculate approximately the rate of heat transfer between an exhaust pipe wall and a gas under unsteady flow conditions [18].

Heat transfer coefficient (h) of Reynold's analogy:

$$h \quad \frac{f}{2} c_{\text{p}} u\rho \tag{46}$$

and the heat transfer rate is:

$$q \quad \frac{2 fuc_{\text{p}} (T_{\text{w}} \quad T_{\text{g}})}{D} \tag{47}$$

Using this relation and $c_{\text{p}} = [k/(k-1)]R$, the heat transfer term for the characteristic:

$$(\delta\lambda)_{\text{heat transfer}} \quad \frac{(k\ 1)^2}{2} \frac{qx_{\text{ref}}}{a_{\text{ref}}^3} \frac{1}{A} \text{d}Z \tag{48}$$

and for the path line characteristic:

$$(\delta A_{\text{a}})_{\text{heat transfer}} \quad k \frac{A_{\text{a}}}{A^2} U \frac{x_{ref}}{D} \frac{fR}{a_{\text{ref}}^2} (T_{\text{w}} \quad T_{\text{g}}) \text{d}Z \tag{49}$$

Numerical solution on non-homentropic equations

For the right and left running characteristics [18], λI and λII symbols are used respectively.

If X is taken positive form the left to the right

$$\lambda \text{I} = \lambda, \quad \lambda \text{II} = \beta$$

and if X is positive from the right to the left

$$\lambda \text{I} = \beta, \quad \lambda \text{II} = \lambda$$

Using these notations, and $A = (\lambda + \beta)/2$; and $U = (\lambda - \beta)/(k-1)$ a general compatibility equation can be expressed as:

$$\begin{aligned} \text{d}\lambda \quad & \frac{\lambda \quad \beta}{2A_{\text{a}}} \text{d}A_{\text{a}} \quad \frac{(k\ 1)^2}{\lambda \quad \beta} \frac{qx_{\text{ref}}}{a_{\text{ref}}^3} \text{d}Z \quad \frac{(\lambda \quad \beta)(\lambda \quad \beta)}{4} \frac{1}{F} \frac{\text{d}F}{\text{d}X} \text{d}Z \\ & \frac{k\ 1}{2} 2f \frac{x_{\text{ref}}}{D} \frac{(\lambda \quad \beta)^2}{(k\ 1)} \frac{\lambda \quad \beta}{|\lambda \quad \beta|} 1 \quad \frac{2(\lambda \quad \beta)}{\lambda \quad \beta} \text{d}Z \end{aligned} \tag{50}$$

We define the ends of the duct as odd and even numbers, then if the nominal slope of the characteristics is in the odd to even end direction $\lambda = \lambda$I and $\beta = \lambda$II in (eq. 43).

If the nominal slope of a characteristics is in the even to odd end direction, then

$$\beta = \lambda \mathrm{I},\ \lambda = \lambda \mathrm{II} \text{ in (eq. 43)}$$

In line with this convention pipes are numbered 1-2, 3-4, *etc*., in fig 2.

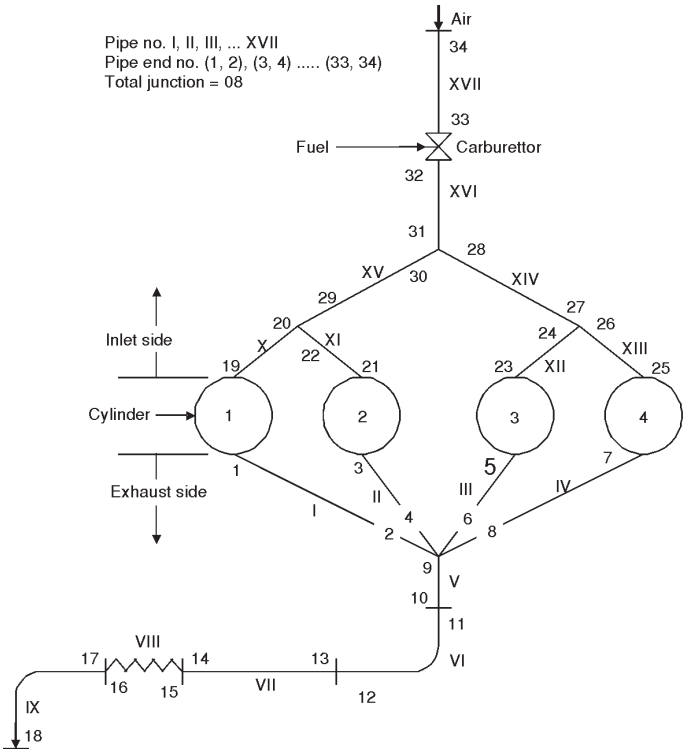

Figure 2. The pipe and pipe end numbers for computational analysis

For path line characteristics, the required λ and β at a path line can be calculated by using linear interpolation between the values at the two mesh points on either side of the path line. The compatibility equation is used which gives the change in entropy δA_{a_k} as:

$$\delta A_{a_k} \quad \frac{k \quad 1}{2} \frac{4A_{a_k}}{(\lambda_k \quad \beta_k)^2} \quad \frac{qx_{ref}}{a_{ref}^3} \quad \frac{2fx_{ref}}{D} \left| \frac{\lambda_k \quad \beta_k}{k \quad 1} \right|^3 \quad \Delta Z \tag{51}$$

Species formation

It is considered that there are 12 species present in the combustion product in the cylinder and in the exhaust. These are H_2O, H_2, OH, H, N_2, NO, N, CO_2, CO, O_2, O, and Ar. These species could reach equilibrium condition if sufficient time is allowed for the reactions to take place under a certain state [17, 18, 20].

Criterion for chemical equilibrium can be expressed by Gibbs function as:

$$(\mathrm{d}G)_{T,p} = 0$$

the specific Gibbs function is expressed as:

$$\frac{g(T)}{\bar{R}T} \quad a_g(1 \quad \ln T) \quad b_g T \quad \frac{c_g}{2}T^2 \quad \frac{d_g}{3}T^3 \quad \frac{e_g}{4}T^4 \quad k_g \tag{52}$$

where a_g, b_g, c_g, d_g, e_g, and k_g are constants. Their values are obtained from reference [17, 18, 20].

Considering the equilibrium equation of reaction used by Vickland *et al*. [17, 18]:

$$\upsilon_a A + \upsilon_b B \rightleftharpoons \upsilon_c C + \upsilon_d D \tag{53}$$

The equilibrium constant K_p is obtained by:

$$K_p \quad \frac{X_c^{\upsilon_c} X_d^{\upsilon_d}}{X_a^{\upsilon_a} X_b^{\upsilon_b}} p^{\upsilon_c \quad \upsilon_d \quad \upsilon_a \quad \upsilon_b} \tag{54}$$

where υ is the stoichiometric coefficient, X – the molar fraction, and p – the total pressure.

The equilibrium constants for all chemical equilibrium equations are obtained by using the following relation:

$$\ln K_p \qquad \frac{\upsilon g(T)}{\bar{R}T}_{\text{reactant}} \qquad \frac{\upsilon g(T)}{\bar{R}T}_{\text{product}} \qquad \frac{\Delta H_0}{\bar{R}T} \tag{55}$$

NO formation

It is observed that the formation of NO and CO in the cylinder and in the exhaust is not in equilibrium. The rate kinetics of NO is considered in the present work. The seven governing equations for NO formation are considered on the theory developed by Lavoie *et al*. [11, 17, 18].

The first equation is:

$$\mathrm{N} + \mathrm{NO} \rightleftharpoons \mathrm{N_2} + \mathrm{O} \tag{56}$$

For the eq. (56):

$$\frac{1}{V}\frac{d}{\mathrm{d}t}[(\mathrm{NO})V] \qquad K_{1f}[\mathrm{N}][\mathrm{NO}] \quad K_{1b}[\mathrm{N_2}][\mathrm{O}] \tag{57}$$

where K_{1f} = forward rate constant ($K_{1f} = 3.1\cdot10^{10}\mathrm{e}^{-160/T}$), K_{1b} = backward rate constant, V = volume of burned gas, and K_{1b} is obtained by using the relation:

$$K_{1f}[\mathrm{N}]_e[\mathrm{NO}]_e = K_{1b}[\mathrm{N_2}]_e[\mathrm{O}]_e = R_1 \tag{58}$$

The following rate equation for NO is obtained [15]:

$$\frac{1}{V}\frac{d}{\mathrm{d}t}[(\mathrm{NO})V] \quad 2(1 \quad \alpha_e^2) \quad \frac{R_1}{1 \quad \alpha_e \dfrac{R_1}{R_2 \quad R_3}} \quad \frac{R_6}{1 \quad \dfrac{R_6}{R_4 \quad R_5 \quad R_7}} \tag{59}$$

where $\alpha_e = [\mathrm{NO}]/[\mathrm{NO}]_e$ and "e"'represents the equilibrium condition.

CO formation

The formation of carbon monoxide inside the cylinder is assumed to be at equilibrium condition up to the peak value. After that the concentration of CO is assumed to lie between peak equilibrium and current equilibrium value, because at lower temperature during expansion process, the actual chemical reaction rates for the formation of CO lag behind the equilibrium value leading to a higher value than obtained at equilibrium [18, 22]. A multiplication factor called COFAC is introduced to obtain the correct value at the exhaust.

The following relation is used for the computation work:

$$XCO = XCO_{eq} + COFAC(XCO_{max} - XCO_{eq}) \quad (60)$$

where XCO = concentration of corrected CO, XCO_{eq} = concentration of CO at equilibrium, XCO_{max} = maximum value of CO concentration at equilibrium condition, and COFAC = scale factor lies between 0 and 1; 0 means the instantaneous equilibrium value of CO, and 1 means CO is frozen at the peak value.

Presentation and discussion of results

The fuel and air mixture inducted through the inlet valve into the engine cylinder, where it mixes with residual gas, and then the mixture is compressed. The combustion is initiated during the compression stroke at 33.6° before TDC by electric discharge of a spark plug. As the flame continues to grow and propagates across the combustion chamber, the pressure rapidly rises and reaches a maximum just after TDC, and then decreases during the remainder of expansion stroke as shown in fig. 3(a), (b), (c) for different equivalence ratios, 0.88 , 1.05, and 1.1, re-

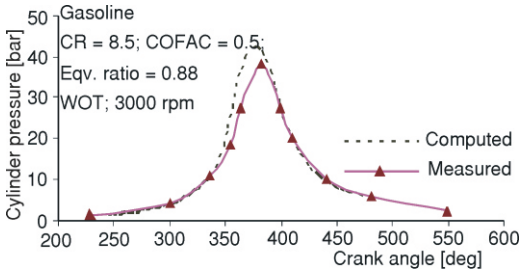

Figure 3(a) Computed and measured cylinder pressure *vs*. crank angle (eqv. ratio = 0.88)

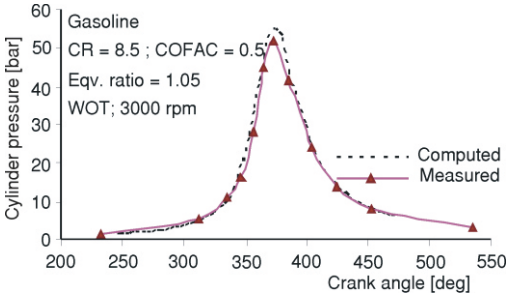

Figure 3(b) Comparison of measured and computed cylinder pressure *vs*. crank angle (eqv. ratio = 1.0)

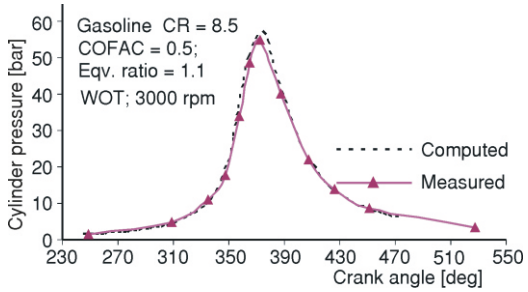

Figure 3(c) Comparison of measured and computed cylinder pressure *vs*. crank angle (eqv. ratio = 1.1)

spectively. As in figures, the predicted results have been validated by comparison with experimental results obtained from Vauxhall Victor 2000cc, four cylinders, four stroke SI engine. The technical data for the engine are given in tab. 1.

Referring to fig. 3(a), (b), and (c) the computed curves follow the experimental cylinder pressure curves, but the measured and computed peak pressures are slightly different.

The discrepancy of the peak pressure is caused by the cycle to cycle dispersion, and is due to non-homogeneity of fuel mixture and supply in the cylinder in actual case, but theoretical calculations are based on constant homogeneous mixture supply at every cycle. A great deal of experimental research work [21, 23] has been done on cyclic dispersion. Another major source of cycle to cycle variation is due to the variation in the spherical burning area produced by variation in the position of the wall contact flame center and variation in the laminar flame speed at the spark and fluctuation in the first eddy burn [24, 25].

The prediction of indicated mean effective pressure (IMEP) is shown in fig. 4. IMEP reduces throughout the higher speed and lower range and maximize in the engine's mid range. At higher and lower engine speed range volumetric efficiency decreases which causes lower IMEP.

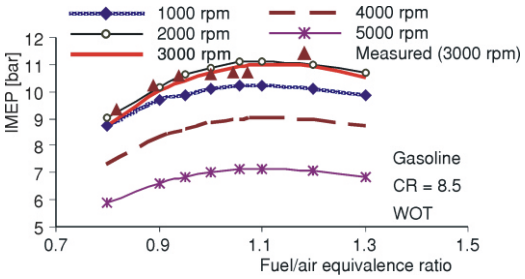

Figure 4. Variation of indicated mean effective pressure with fuel/air equivalence ratio and engine speed

Predicted values are good in agreement with experimental values at 3000 rpm. Experimental values are given in reference [18]. IMEP gradually increases with equivalence ratio and reaches maximum at slightly enriched stoichiometric mixture (between $\Phi = 1$ to 1.1). Due to dissociation, at high temperatures following combustion, molecular oxygen is present in the burned gases under stoichiometric condition, so more additional fuel can be added and partially burned. This increases the temperature and the number of moles of the burned gas in the cylinder. These effects increase the pressure to give increased mean effective pressure and indicated power. Above this equivalence ratio ($\Phi > 1.0$), power decreases due to the decreasing combustion efficiency, because of insufficient air for com-

Table 1.

Engine type (SI)	Vauxhall Victor 2000cc
Cycle	4 stroke
Number of cylinder	Four cylinder in line
Cylinder bore	9.53 cm
Stroke	6.92 cm
Connecting rod length	13.65 cm
Compression ratio	8.5
Angle of ignition	33.60 bTDC
Valve timing	
– evo	114.60 aTDC
– evc	393.60 aTDC
– ivo	326.60 aTDC
– ivc	605.40 aTDC
Spark plug position from nearest point of wall/bore (ND)	0.3517
Firing order	1-3-4-2
Fuel	Gasoline (C_7H_{13})
Calorific volue	44 MJ/kg
Internal energy coefficients	
– u2	–1.0715e4
– u3	2.89500e2
– u4	–0.800e–1
– u5	1.66500e–5

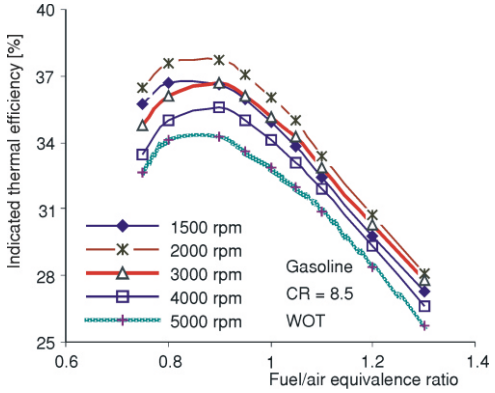

Figure 5. Variation of indicated thermal efficiency with fuel/air equivalence ratio and engine speed

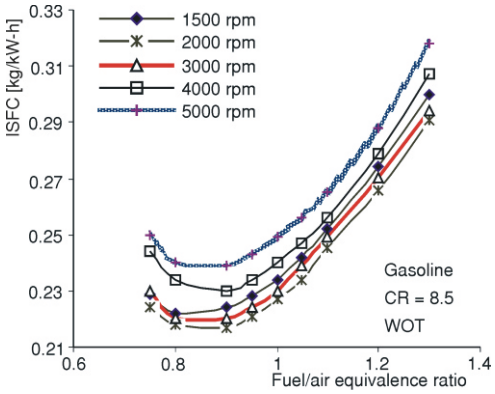

Figure 6. Variation of indicated speed fuel consumption with fuel/air equivalence ratio and engine speed

plete combustion of fuel. The same factors mention above are influenced in the variation of thermal efficiency for equivalence ratio and engine speed range, as shown in fig. 5.

For mixtures lean of stoichiometric, the fuel conversion efficiency increases linearly as Φ decreases below 1.0. Combustion of mixtures leaner than stoichiometric produces products at lower temperature, and with less dissociation of the triatomic molecules CO_2 and H_2O.Thus the fraction of chemical energy of fuel is released as sensible energy near TDC is greater, which is transferred as work to the piston and efficiency becomes higher.

The effect of fuel-air equivalence ratio on indicated specific fuel consumption (ISFC) of engine at different speed range is shown in fig. 6. ISFC varies little over the engine speed range; this variation of ISFC is due to the volumetric efficiency and fuel conversion efficiency. As the figure shows the engine is most efficient when running stoichiometric or slightly lean and mid range of speed, just below 3000 rpm. At very lean mixture engine wastes fuel because of misfire, and rich mixture it wastes fuel since there is not enough oxygen present to liberate all of the fuel's energy.

The effect of variation in the equivalence ratio on NO emission is shown in fig. 7. NO forms throughout the high temperature burned gasses behind the flame through chemical reactions involving nitrogen and oxygen atoms and molecules, which do not attain chemical equilibrium. The higher the burned gas temperature the higher is the rate of formation of NO. As the burned gases cool during expansion stroke the reactions involving NO freeze. Maximum burned gas temperatures occur at slightly enriching of stoichiometric; however, at this equivalence ratio oxygen concentrations are low, resulting low NO concentration level. As the mixture is enriched, burned gas temperature falls, and as the mixture is leaned out increasing oxygen concentration initially offsets the falling gas temperature and NO emissions attain peak value at Φ 0.9. Near the stoichiometric and peak value of computed NO agrees with experimental values, as shown in fig. 7. But there are some difference in peak value as recorded in the same figure. This difference is expected be-

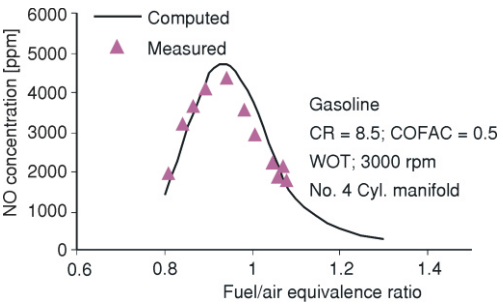

Figure 7. Variation of NO concentration with fuel/air equivalence ratio

cause the computed results are obtained with the assumption of constant homogeneous mixture supply.

The variation of CO emission with the equivalence ratio is shown in fig. 8. With rich equivalence ratio there is insufficient oxygen to burn all the carbon fully in the fuel to CO_2. Also, in the high temperature products even with lean mixtures, dissociation ensures there is significant CO level. Later in expansion stroke, the CO oxidation process also freezes as the burned gas temperature falls. The CO emissions were predicted with the assumption that CO after achieving the peak equilibrium in cylinder maintains an arithmetic mean value of peak equilibrium and existing equilibrium value (COFAC = 0.5). The computational values match closely with the experimental values.

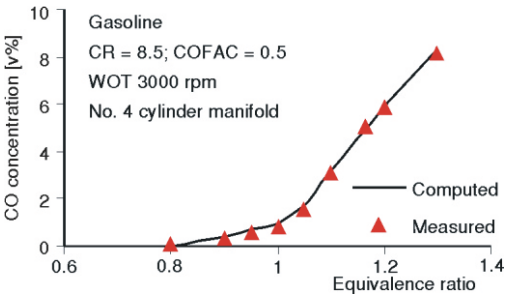

Figure 8 Variation of CO concentration with fuel/air equivalence ratio

At the exhaust valve outlet, pressure and temperature are varied with crank angle as shown in figs. 9 and 10, respectively. 0° crank angle is marked when the cylinder no. 1 is at TDC and expansion stroke begins. The exhaust process begins at 65.4° before BDC and closes at 36.6° after TDC. The exhaust gas pressure and temperature are increased sharply during blow-down period and slowdown towards TDC and then continuous up to BDC. It is so because, when the exhaust valves open the violent blow-down generates a strong pressure pulse which travels down to the exhaust pipe at sonic velocity and expands into the exhaust pipe.

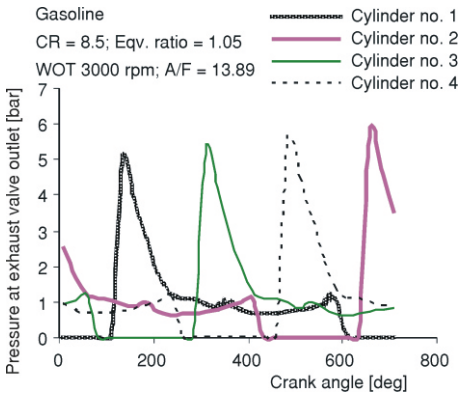

Figure 9. Four cylinder outlet pressure *vs.* crank angle

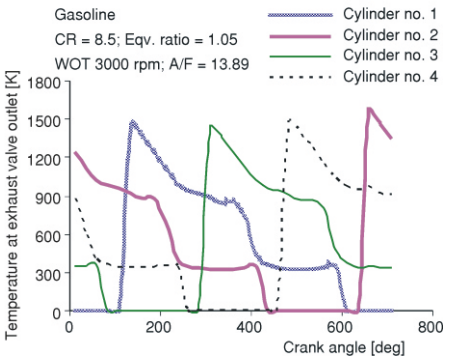

Figure 10. Four cylinder outlet temperature *vs.* crank angle

The exhaust manifold pressure and temperature depend upon the inlet manifold pressure and speed of the engine. The pressure in the inlet manifold varies during each cylinder's intake process due to the variation in piston speed, valve open area and the unsteady gas flow. The pulsating exhaust flow from each cylinder's exhaust process sets-up pressure waves in the exhaust pipe. Figures 11 and 12 show the measured and computed pressure variations at upstream

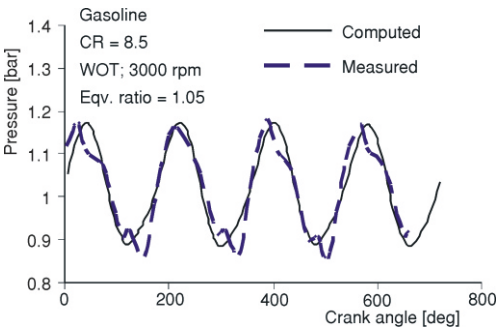

Figure 11. Comparison of computed and measured pressure at upstream pipe no. VII

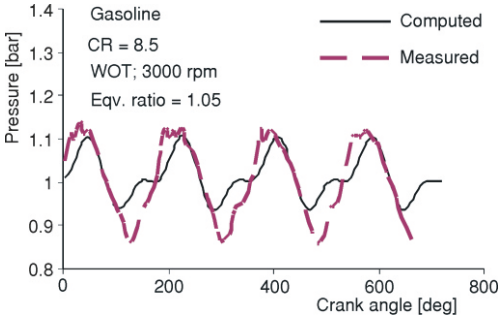

Figure 12. Comparison of computed and measured pressure at downstream pipe no. VII

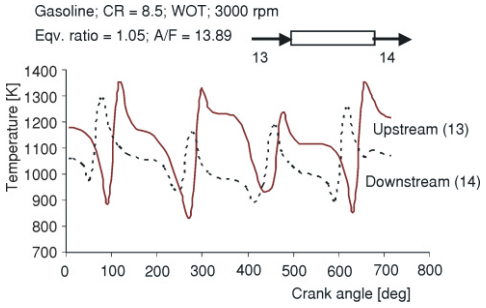

Figure 13. Temperature at upstream and downstream of pipe no. VII end *vs.* crank angle

and downstream of pipe no. VII, respectively. The two results are in agreement. Figure 13 shows the computed results of temperature variation at upstream and downstream of pipe no. VII.

As the pressure and temperature diagrams are obtained in a four cylinder engine exhaust system, the four primary pulses are associated with the exhaust system blow down. The timing of the pulses follows the firing order of the cylinders and the phasing is due to the relative position of one cylinder to another.

Conclusions

A computer simulation technique has been developed to model the gas dynamics phenomena which occur in the intake and exhaust manifolds of multi-cylinder spark ignition engines. The exhaust system has a critical effect on the charging and gas exchange process and hence on the overall performance of the engine. This arises from the cycle of events during the exhaust and recharging phases when the exhaust pipe and induction manifold are both open to the cylinder at the same time. In the development of internal combustion engine attention is drawn to the pressure phenomena occurring in the exhaust pipe.

Exhaust pulses affect the engine performance both in timing of the pulse and overall length of the pipe. The influence of the pressure pulses on the charging process affects the overall performance of the engine. Exhaust system should be designed to enhance the engine performance.

The theoretical results obtained from the present model and experimental results obtained from a four cylinder, four stroke Vauxhal-Victor 2000cc petrol engine have confirmed the reliability and accuracy of the present model for predicting the performance of SI engine running on gasoline fuel.

The present model can be used to examine the effect of fuel type, engine geometry, and operation parameters on combustion cycle and engine performance. The only change required in the model to allow for other fuel is to use different internal energies of reaction and thermodynamics data for the fuel. In addition, formulations for the flame speed are required for different fuels.

Nomenclature

A – non-dimensional speed of sound (=a/a_{ref})
A_a – non-dimensional form of a_A (=a_A/a_{ref})
a – speed of sound, [ms^{-1}]
a – Annand constant for convective heat transfer (in eq. 3)
a_A – speed of sound after isentropic change of state to reference pressure, [ms^{-1}]
a_g, b_g, c_g, d_g, e_g, k_g – polynomial coefficients of gas
a_{ref} – reference speed of sound, [ms^{-1}]
b – Annand constant for heat transfer (in eq. 3)
CR – compression ratio
CV – calorific value of fuel, [kJkg^{-1}]
c – radiation heat transfer coefficient (= $4.3\cdot10^{-9}$ [kWT^{-4}m^{-2}])
c_v – specific heat of gas at constant volume, [kJkg^{-1}K^{-1}]
D – diameter, [m]
D – diffusion coefficient (diffusivity), [cm^{2}s^{-1}]
F – area, [m^2]
F_f – flame factor
f – friction factor (= $\tau_w/0.5\,\rho u^2$)
f_i – fraction fresh mixture
g – specific Gibbs free energy function
H_0 – enthalpy at absolute zero, [kJ]
h_0 – specific enthalpy at absolute zero, [kJkg^{-1}]
h_r – heat transfer coefficient of Reynolds' analogy, [Wm^{-2}K^{-1}]
K_{1b} – backward rate constant
K_{1f} – forward rate constant
K_p – equilibrium constant
k – specific heat ratio (= cp/cv)
k_q – thermal conductivity (= $c_p\mu/0.7$) [kJs^{-1}m^{-1}K^{-1}]
m – mass, [kg]
p – pressure, [Nm^{-2}]
Q – total heat flux, [kJ]
q – rate of heat transfer per unit time per unit mass of fluid, [kW]
R – gas constant, [kJkg^{-1}K^{-1}]
$\overline{R}$ – universal gas constant, [kJkmol^{-1}K^{-1}]
Re – Reynolds number
R_i – one way equilibrium rate for equation (i = 1, 2, 3, 4, 5, 6, 7)
RPM – revolution per minute
r – flame radius, [m]
T – gas temperature, [K]
T_m – unburned mixture temperature, [K]
T_p – burned or product temperature, [K]
T_w – temperature of pipe wall, [K]
t – time, [s]
U – internal energy, [J]
U – non-dimensional particle velocity (= u/a_{ref})
u – particle velocity, [ms^{-1}]
u – specific internal energy, [Jkg^{-1}] (in tab. 1)
u_f – laminar flame speed, [ms^{-1}]
u_t – turbulent flame speed, [ms^{-1}]
V – volume, [m^3]
W – work, [W]
X – non-dimensional length (= x/x_{ref})
x – distance, [m]
x_i – molar fraction of i^{th} species
x_{ref} – reference length, [m]
Z – non-dimensional time (= $a_{ref}.t/x_{ref}$)

Greek letters

α – crank angle, [deg]
β – Riemann variable (A – U(k –1)/2)
$\Delta\theta$ – delay period, [deg]
λ – Riemann variable (A + U(k – 1)/2)
μ – viscosity of gas, [kgm^{-1}s^{-1}]
ρ – gas density, [kgm^{-3}]
τ_w – wall shear stress, [Nm^{-2}]
υ – stoichiometric coefficient
Φ – equivalence ratio

Subscripts

0 – stagnation condition
c – cylinder
e – exhaust
g – gas
i – inlet
K – path line count
m – unburned mixture
n – previous time step
n+1 – current time step
p – product (burned)
ref – reference
u – unburned
w – wall

References

[1] Abd Alla, G. H., Computer Simulation of a Four Stroke Spark Ignition Engine, *Energy Conversion and Management, 43* (2002), 8, pp. 1043-1061
[2] Kodah, Z. H., *et al*. Combustion in a Spark-Ignition Engine, *Applied Energy, 66* (2000), 3, pp. 237-250
[3] Mustafi, N. N., *et al*., Spark-Ignition Engine Performance with 'Powergas' fuel (Mixture of CO/H_2): A Comparison with Gasoline and Natural Gas, *Fuel 85* (2006), 12-13, pp. 1605-1612

[4] Bayraktar, H., Durgun, O., Investigation the Effect of LPG of on Spark Ignition Engine Combustion and Performance, *Energy Conversion and Management 46* (2005), 13-14, pp. 2317-2333
[5] Kutlar, O. A., Arslan, H., Calik, A. T., Method to Improve Efficiency of Four Stroke, Spark Ignition Engines at Part Load, *Energy Conversion and Management, 46* (2005), 20, pp. 3202-3220
[6] Adams, *W. H., et al*., Analysis of the Combustion Process of a Spark Ignition Engine with a Variable Comression Ratio, SAE paper no. 870610, 1988
[7] Hamdan, M. A., Al-Subaih, T. A., Improvement of Locally Produced Gasoline and Studying its Effect on Both the Performance of the Engine and the Environment, *Energy Conversion and Management, 43* (2002), 14, pp. 1811-1820
[8] Yamin, J. A., Badran, O. O., Analytical Study to Minimize the Heat Losses from Propane 4 Stroke Spark Ignition Engine, *Renewable Energy, 27* (2002), 3, pp. 463-478
[9] Kesgin, U., Study on the Design of Inlet and Exhaust System of a Stationary Internal Combustion Engine, *Energy Conversion and Management, 46* (2005), 13-14, pp. 2258-2287
[10] Bayraktar, H., Durgun, O., Mathematical Modeling of Spark Ignition Engine Cycle, *Energy Source, 25* (2003), 7, pp. 651-666
[11] Al-Baghdadi, M. A. R. S., Al-Janabi, H. A.-K., Improvement of Performance and Reduction of Pollutant Emission of a Four Stroke Spark Ignition Engine Fueled with Hydrogen-Gasoline Fuel Mixture, *Energy Conversion and Management 41* (2000), 1, pp. 77-91
[12] Al-Baghdadi, M. A. R. S., A Simulation Model for Single Cylinder Four- Stroke Spark Ignition Engine Fueled eith Alternative Fuels, *Turkish J. Eng. Env. Sci., 30* (2006), 6, pp. 331-350
[13] Verhelet, S., Sierens, R., A Quasi-Dimensional Model for the Power of a Hydrogen-Fuelled ICE, *International Journal of Hydrogen Energy, 33* (2007), pp. 4755-4762
[14] Bayraktar, H., Theoritical Investigation of Flame Propagation Process in an SI Engine Running on Gasoline Ethanol Blends, *Renewable Energy, 32* (2007), 4, pp. 758-771
[15] Winterbone, D. E., Pearson, R. J., A Solution of the Wave Equations Using Real Gases, *Int. J. Mech. Sci., 34* (1992), 12, pp. 917-932
[16] Zhang, G. Q., Assanls, D. N., Manifold Gas Dynamics and Its Coupling with Single Cylinder Engine Models Using Simulink, *Journal of Engineering for Gas Turbine and Power, 125* (2003), 3, pp. 563-571
[17] Heywood, J. B., Internal Combustion Engine Fundamental, McGraw-Hill, New York, USA, 1989
[18] ***, Thermodynamics and Gas Dynamics of Internal Combustion (Eds. J. H. Horlock, D. E., Winterbone), Voll. II, Clarendon, Oxford, UK, 1986
[19] Shaver, G. M., Roelle, M. J., Gerdes, J. C., Modeling Cycle-to-Cycle Dynamics and Mode Transition in HCCI Engine with Variable Valve Actuation, *Control Energy Practice, 14* (2006), 3, pp. 213-222
[20] Turns, S. R., An Introduction to Combustion, McGraw-Hill, New York, USA, 2000
[21] Zervas, E., Correlation Between Cycle to Cycle Variation and Combustion Parameters of Spark Ignition Engine, *Applied Thermal Engg, 24* (2002), 1, pp. 2073-2081
[22] Sher, E., Bar-Kohany, T., Optimization of Variable Valve Timing for Maximizing Performance of an Unthroattle SI Engine – a Theoretical Study, *Energy, 27* (2002), 5, pp. 757-775
[23] Ceviz, M. A., Yuksel, F., Cyclic Variation on LPG and Gasoline-Fuelled Lean Burned SI Engine, *Renewable Energy, 31* (2006), 12, pp. 1950-1960
[24] Keck, J. C., *et al*., Early Flame Development and Burning Rates in Spark Ignition Engine and Their Cycle Variability, SAE paper no. 870164, 1988
[25] Kalghatgi, G. T., Spark Ignition, Early Flame Development and Cycle Variation in I. C. Engines; SAE paper no. 870163, 1988

Authors' affiliation:

J. V. Tirkey (**corresponding author**)
Institute of Technology, Mechanical Engineering Department,
Banaras Hindu University, Varanasi, 221005-INDIA
E-mail: jvtirkey@yahoo.co.in, jvtirkey@gmail.com

H. N. Gupta, S. K. Shukla
Institute of Technology, Mechanical Engineering Department,
Banaras Hindu University, Varanasi, 221005-INDIA

Paper submitted: December 17, 2009
Pper revised: March 8, 2009
Paper accepted: May 30, 2009